IEEE Photonics Journal
An IEEE Photonics Society Publication

Open Access

Backward-Emitting Silicon Nitride Optical Phased Array Enabling Efficient Wavelength-Tuned Beam Steering

Volume 12, Number 5, October 2020

Chul-Soon Im
Bishal Bhandari
Sung-Moon Kim
Min-Cheol Oh
Kyeong-Pyo Lee
Taehoon Kim
Sang-Shin Lee

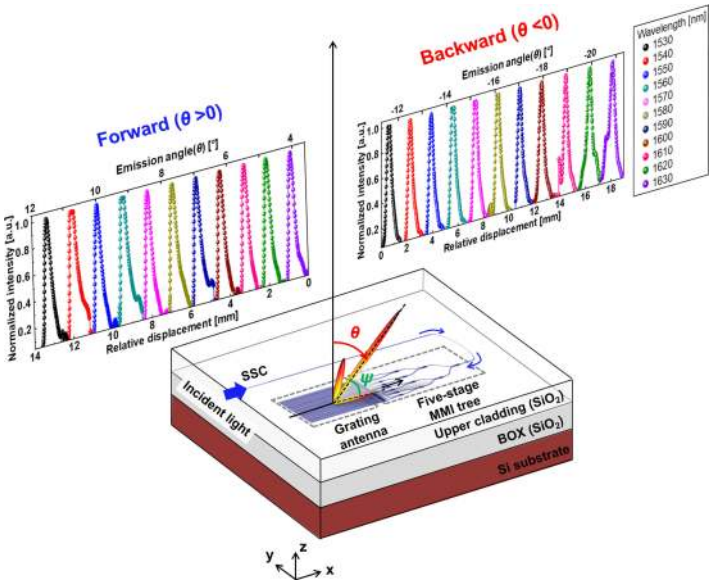

DOI: 10.1109/JPHOT.2020.3019060

Backward-Emitting Silicon Nitride Optical Phased Array Enabling Efficient Wavelength-Tuned Beam Steering

Chul-Soon Im,[1] Bishal Bhandari,[1] Sung-Moon Kim,[2] Min-Cheol Oh,[2] Kyeong-Pyo Lee,[3] Taehoon Kim,[4] and Sang-Shin Lee[1]

[1]Department of Electronic Engineering, Kwangwoon University, Seoul 01897, South Korea
[2]Department of Electronics Engineering, Pusan National University, Pusan (Busan) 46241, South Korea
[3]i3system, Daejeon 34113, South Korea
[4]Agency for Defense Development, Daejeon 34186, South Korea

DOI:10.1109/JPHOT.2020.3019060

Manuscript received June 27, 2020; accepted August 20, 2020. Date of publication August 25, 2020; date of current version September 15, 2020. This work was supported by the Agency for Defense Development (ADD), Korea under Grant UE171060RD and Kwangwoon University in 2020. Corresponding author: Sang-Shin Lee (email: slee@kw.ac.kr).

Abstract: Silicon nitride (SiN) optical phased arrays (OPAs) have emerged as a potential alternative to their silicon counterparts, due to their potential use in enhanced solid-state light detection and ranging. Grating antennas based on a SiN waveguide suffer from a limited beam steering efficiency, owing to the relatively lower effective refractive index of the waveguide. To mitigate this limitation, we propose and demonstrate a backward-emitting SiN OPA incorporating a reinforced grating vector, which provides efficient wavelength-tuned beam steering along the longitudinal direction. Two backward-emitting OPAs were primarily characterized by their steering efficiency and the spectral emission for the main lobe, and they were compared with a forward-emitting device using a weakened grating vector. The results indicated that strengthening the grating vector for the antenna improved the beam steering efficiency but adversely affected the dependence of its directionality on the wavelength. The directionality was particularly inspected, with respect to major design parameters for the grating antennas, including the pitch and etch depth of a SiN grating, as well as the thickness of a buried oxide and SiN core layer. The proposed backward-emitting OPA scheme is expected to significantly promote its feasibility as an advanced beam scanning device.

Index Terms: Optical phased array, light detection and ranging, silicon nitride photonics.

1. Introduction

Optical phased arrays (OPAs) in silicon were extensively studied to realize a beam steering system based on photonic integrated circuits (PICs) [1]. Advanced one-dimensional OPA circuits on a Si platform have demonstrated advantageous features for free-space beam steering, owing to their compatibility with complementary metal oxide semiconductor (CMOS) processes and high index contrast to silicon dioxide. Si OPAs may be a viable replacement for their mechanical counterparts, which are reliant on a micro-machined or motor-driven mirror [2]–[9]. Recently, the feasibility of such an OPA has been further increased by the development of a superior cost-effective laser,

exhibiting a high optical power of 21 dBm over a broad spectral range [10]. However, the high index contrast of Si waveguides requires precise fabrication to create Si-based PICs [11], [12], which makes them vulnerable to fabrication errors. Furthermore, the large third-order nonlinearity in telecommunication bands makes Si OPAs unsuitable for the long-range transmission required for light detection and ranging (LiDAR) and data communications [11]–[13]. As a CMOS-compatible platform, silicon nitride (SiN) photonics has emerged as a potential alternative to Si photonics. Based on the advantageous features of SiN, including a relatively low index contrast, low propagation loss, broad transparent band, and low nonlinearity [11], [14], a large-scale SiN nanophotonic phased array was developed, which emitted a high-quality beam, exhibiting a maximum beam power of approximately 400 mW [15]. Considerable effort was also expended to deal with the low thermo-optic coefficient of SiN [11], [16], by incorporating thermo-optic modulators with a long heating element [17]. However, there has been no report on the wavelength-tuned beam steering of SiN OPAs in the longitudinal direction. Recently, we proposed and characterized wavelength-tuned beam steering in terms of the angular beam steering and emission response [18]. Compared to Si OPAs [4]–[9], the prepared SiN OPA provided a limited steering efficiency of 0.074 °/nm, due to the lower effective index of the waveguide. Despite the notable benefits of the SiN platform, a low steering efficiency would devaluate its potential for beam scanning applications. Thus far, a grating antenna has been designed to radiate light, either nearly vertically or at a slightly slanted angle in the forward direction [3]–[9], [15]. While several studies attempted to develop the emission behavior in the lateral direction [5], [19], [20], the waveguide gratings constituting the antenna have not been suitably designed for beam steering efficiency in the longitudinal direction. To materialize the benefits of using a SiN platform, a design strategy, leading to a highly efficient SiN OPA, should be established.

In this paper, a backward-emitting SiN OPA, which incorporates waveguide grating antennas that serve as a strong grating vector, has been proposed to enhance beam steering efficiency. An investigation of the wavelength-tuned beam steering range of the antenna via a K-space diagram showed that a backward beam emission was advantageous for enhancing the steering efficiency, without incurring undesired higher-order diffraction. For two backward-emitting devices, the beam steering was characterized in terms of the steering range and the directionality, for a wavelength range of 1530–1630 nm, and compared with a forward-emitting device. With the lower effective index of the SiN waveguide, phase variations across the antenna channels were minimized, allowing for a well-defined beam. While the backward-emitting scheme allowed SiN OPAs to provide an enhanced steering efficiency, its strong grating vector made the emission response vulnerable to changes in wavelength. We meticulously analyzed the emission response of the backward-emitting OPAs by inspecting the influence of design parameters, including the period and etching depth of the grating and the thickness of the buried oxide and SiN waveguide layer. The proposed backward-emitting OPA, based on SiN waveguide gratings, is believed to enhance their feasibility as a potential beam-steering platform.

2. Proposed Backward-Emitting SiN OPA

Fig. 1(a) depicts the configuration of the proposed backward-emitting SiN OPA, which is comprised of a spot size converter (SSC), multiple stages of 1×2 multimode interference (MMI) splitters, and a backward-emitting grating antenna. A U-shaped layout was adopted to facilitate the measurement of the backward beam emission at a negative angle of θ. The OPA device was fabricated by depositing a 500 nm-thick SiN film on a 4.0 μm buried oxide (BOX) layer via low pressure chemical vapor deposition, used to alleviate the optical loss of SiN waveguides [11], [14]. The SiN layer was fully etched to pattern the waveguides. A 3.1 μm-thick oxide film was subsequently deposited via plasma enhanced chemical vapor deposition to form the upper cladding. A microscope image of the fabricated backward-emitting OPA is shown in Fig. 1(b). Transverse electric polarized light was launched into a 2.0 μm-wide waveguide via the SSC. After being transmitted through the U-shaped waveguide, the light was evenly divided into two channels by each MMI splitter; the specific arrangement was designed to create an MMI region, with dimensions of 7.0×29.5 μm^2.

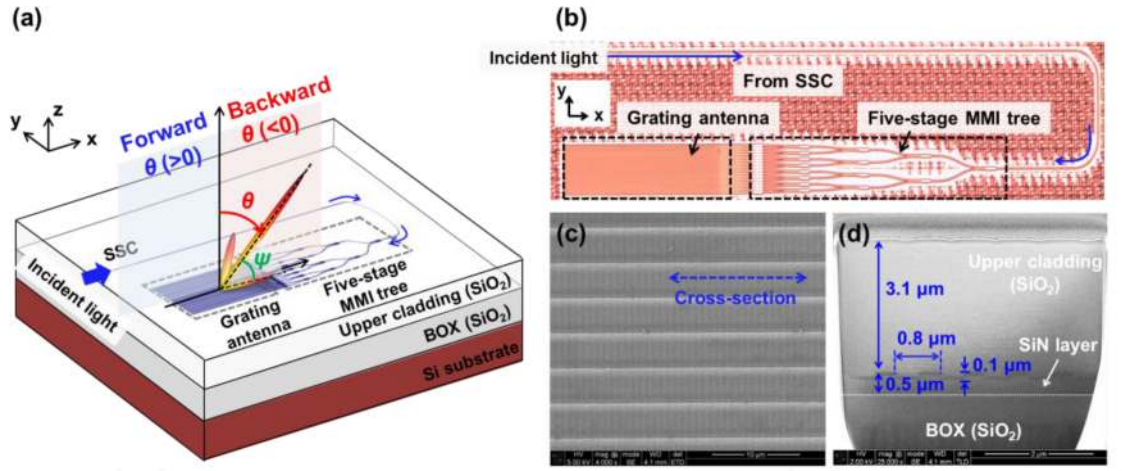

Fig. 1. (a) Proposed U-shaped SiN OPA executing backward beam radiation. (b) Microscope image of the fabricated backward-emitting OPA. SEM images of (c) the antenna and (d) its cross-section along the propagation direction.

The light was evenly distributed into 32 channels by means of the five-stage MMI tree. The channels were uniformly spaced, according to a pitch of 4.0 μm. The bent waveguides and MMI splitters were appropriately placed to impose an equivalent phase condition on each of the array channels; thus, a well-defined beam could be formed by the device, requiring no additional phase compensation.

For the backward-emitting antenna, the gratings were produced by partially etching a SiN waveguide, thereby diffracting light into the air at an angle θ in the negative domain. The emission angle was determined by $\sin\theta = n_{eff} - (\lambda/\Lambda_{sg})$, where n_{eff} is the effective refractive index of the fundamental guided mode associated with the grating antenna, Λ_{sg} is the period of the surface-relief grating, and λ is the wavelength in free space. Fig. 1(c) displays a scanning electron microscope (SEM) image of an array of SiN waveguide grating antennas. The gratings were manufactured in a 500 μm long SiN waveguide core to exhibit a uniform depth of about 100 nm and a period of 0.8 μm, thereby inducing beam emission in the backward direction. The SEM image of the cross-section of the manufactured antenna, shown in Fig. 1(d), indicates that the waveguide gratings were faithfully engraved in the SiN core as intended.

To explore the beam steering range, tuned by the wavelength, in the longitudinal direction, light diffraction due to the grating antenna was examined using a K-space diagram [21]. As illustrated in Fig. 2(a), the grating antenna was assumed to have a grating vector **G**, the magnitude of which along the x-axis is given by $2\pi/\Lambda_{\mathrm{sg}}$. When the guided mode propagates in the waveguide grating with a propagation constant β ($= n_{\mathrm{eff}} \cdot 2\pi/\lambda$), it diffracts into the air, where the wavenumber $|\mathbf{k}|$ corresponds to $2\pi/\lambda$. The angle of diffraction θ is governed by the phase-matching condition between the propagation constant of the waveguide mode β and the grating vector **G**. The achievable steering range ($\Delta\theta$) is determined by two diffracted waves, the wavenumbers of which are given by $|k_1|$ and $|k_2|$, as observed at two different wavelengths λ_1 and λ_2 ($\lambda_1 < \lambda_2$), respectively. Here, the propagation constants were assumed to be β_1 and β_2 for λ_1 and λ_2, respectively. With the aid of a finite-difference-time-domain (FDTD) tool, FDTD Solutions (Lumerical Inc., Canada), the angular steering range was investigated by scanning wavelengths between 1530 and 1630 nm, under the refractive indices of SiN and SiO_2 set at 1.97 and 1.44, respectively. As shown in Fig. 2(b), a wide steering range was attained for Λ_{sg}-either smaller than 1.0 μm or larger than 1.5 μm. However, for Λ_{sg} larger than 1.5 μm, the range was restricted because the desired first-order diffraction was not available for $\lambda = 1530$ nm in the upward direction. Moreover, for Λ_{sg} higher than 1.2 μm, a second-order grating lobe appeared for $\lambda = 1530$ nm, incurring an undesired optical loss in the main lobe. Hence, a smaller Λ_{sg} was sought for to extend the steering range under

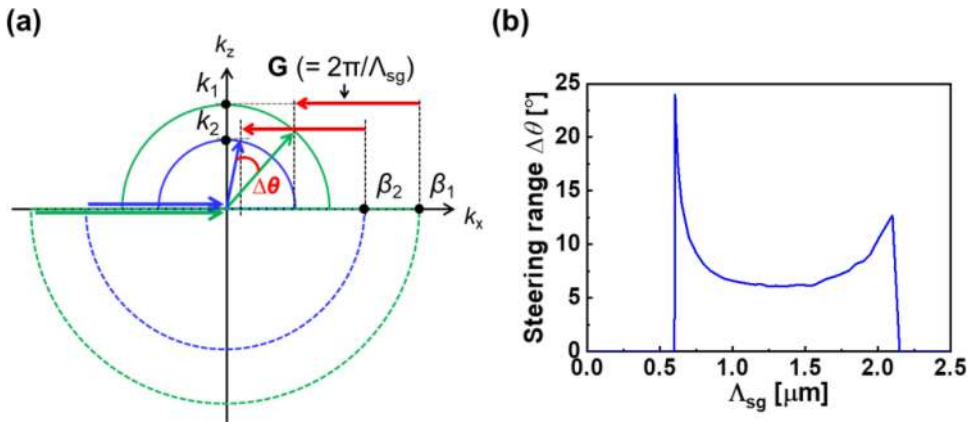

Fig. 2. (a) K-space diagram associated with the grating antenna for two different wavelengths. (b) Expected beam steering range as a function of Λ_{sg} in response to wavelengths varying between 1530 and 1630 nm.

the desired spectral band. To investigate the dependence of the beam steering characteristics on the emission direction, we prepared and compared two OPA candidates based on different grating vectors, which were meant to provide similar radiation in opposite directions for $\lambda = 1550$ nm. A stronger grating vector, corresponding to a 0.8 μm period, was principally selected for the backward-emitting device, whereas a weaker grating vector, resulting from a period of 1.0 μm, was chosen for the forward-emitting case. A SiN OPA with $\Lambda_{sg} = 0.7$ μm was additionally assessed to verify the emission characteristics in the backward direction.

3. Experimental Results

The beam steering performance of the fabricated OPAs was evaluated using the metrics of the angular steering range and the emission efficiency of the main lobe, for wavelengths ranging from 1530 to 1630 nm. An infrared camera (ABA-001IR-GE, AVAL DATA) and a photodiode power sensor (S130C, Thorlabs) were employed to monitor the emitted beam. Prior to checking the beam steering response, the beam quality of the main lobe was assessed by determining its full width at half maximum (FWHM) divergence. As shown in Fig. 3(a), the OPA device was observed to radiate a main lobe, in conjunction with two first-order grating lobes at angles of $\pm$ 22° along the lateral direction. The main lobe was projected onto the camera, and the intensity profile was monitored by varying the distance (*d*) between the device and the camera. Fig. 3(b) shows the displacement of the main lobe in the x-direction, indicating that, for the backward-emitting device with $\Lambda_{sg} = 0.8$ μm, light was emitted at $\theta = -13.3°$ for $\lambda = 1550$ nm. As shown in Figs. 3(c) and 3(d), the device could generate a well-defined beam, the FWHM divergence angles of which were 0.6° and 0.2° in the lateral and longitudinal directions, respectively. For the forward-emitting device, using $\Lambda_{sg} = 1.0$ μm, light was emitted $\theta = +10.0°$ for $\lambda = 1550$ nm, exhibiting an equivalent divergence. To determine the beam steering range, the displacement of the main lobe in the x-direction was measured at $d =$ 10 cm when the wavelength was scanned from 1530 to 1630 nm. Beam profiles at each wavelength were individually normalized and consecutively arranged. The results for $\Lambda_{sg} = 0.8$ μm and 1.0 μm are plotted in Figs. 4(a) and 4(b), respectively. Both the SiN OPA devices successfully executed wavelength-tuned beam steering, requiring no phase compensation. In response to wavelengths varying from 1530 nm to 1630 nm, the backward-emitting OPA routed the beam from $\theta =$ -11.3° to -20.7° along the longitudinal direction, whereas the forward-emitting device exhibited the opposite behavior, steering the beam from $\theta = +11.5°$ to $+4.1°$. Within the same 100 nm wavelength span, the backward-emitting device, with $\Lambda_{sg} = 0.8$ μm, achieved a steering range of $\Delta\theta = 9.4°$, which

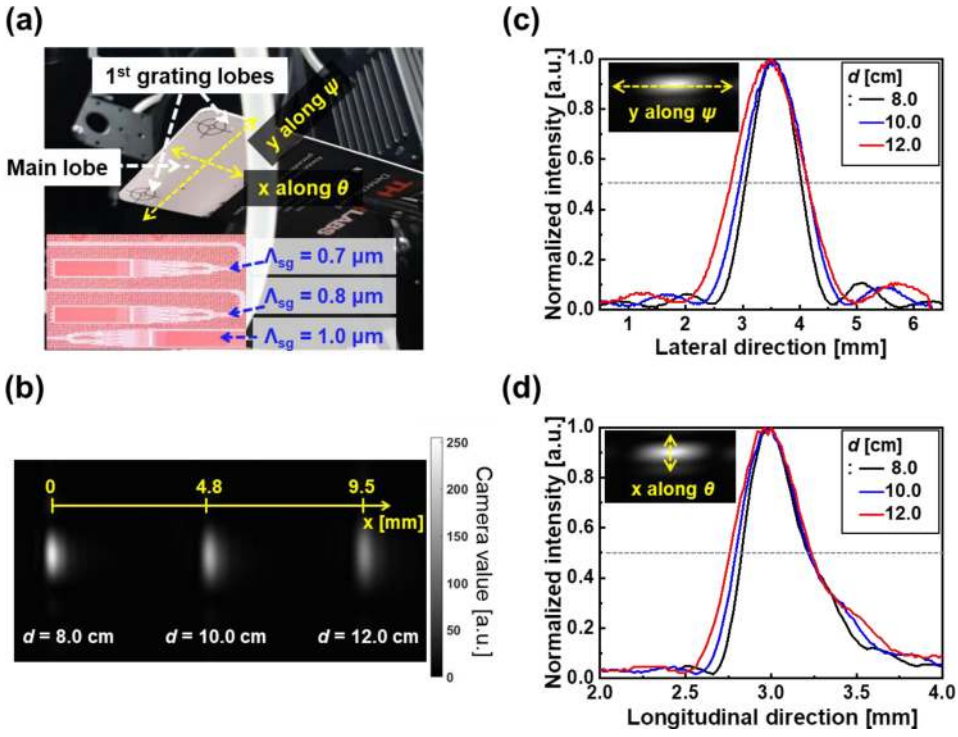

Fig. 3. (a) Measured beam images through an infrared sensor card and a photograph of the three manufactured OPAs. (b) Measured displacement of the main lobe in the x-direction for $\lambda = 1550$ nm, with *d* varying from 8 to 12 cm. Optical intensity profiles along (c) the lateral and (d) longitudinal directions.

resulted in a steering efficiency of 0.094 °/nm. For the forward-emitting case, with $\Lambda_{\mathrm{sg}} = 1.0$ μm, the steering range was $\Delta\theta = 7.4°$, which resulted in a steering efficiency of 0.074 °/nm. These experimental results validated the prediction, based on the K-space diagram, that the steering efficiency of the backward-emitting SiN OPA, for $\Lambda_{\mathrm{sg}} = 0.8$ μm, was 27% better than that of the forward-emitting counterpart, with $\Lambda_{\mathrm{sg}} = 1.0$ μm.

Considering its application as a beam scanning device, the directionality of a beam-radiating antenna should be of prime concern in the context of wavelength-tuned beam steering. The directionality of the antenna was assessed from the total emission efficiency for the main lobe over the desired spectral band. The efficiency of the grating lobes was concurrently investigated to determine the influence of the directionality of the main lobe on the beam steering. The total efficiency alludes to the optical coupling of the corresponding radiating beam from the SSC coupler at $d = 10$ cm. To inspect the characteristics of the main lobe, the measured data were plotted with the simulated results for the upward emission. As illustrated in Fig. 5(a), a two-dimensional (2D) modelled grating antenna, comprising of the BOX, SiN waveguide, and upper cladding, was considered for the simulation. The etch depth (H_{ED}), the thickness of the SiN waveguide core (H_{SiN}), and the thickness of the BOX layer (H_{BOX}) were set to 0.1 μm, 0.5 μm, and 4.0 μm, respectively. As shown in Figs. 5(b) and 5(c), for the main lobe, the two devices exhibited a total efficiency of -6 dB for a wavelength range spanning 1530–1580 nm, which gradually decreased with the increase in wavelength. Based on the results in Figs. 6(a) and 6(b), the total efficiency measured at $\lambda = 1550$ nm could be accounted for by the losses pertaining to the SSC coupling (1.4 dB), the waveguide propagation ($\sim$0.3 dB resulting from 0.4 dB/cm), the five-stage MMI tree (0.5 dB), and the antenna emission (3.8 dB). Compared with the case of $\Lambda_{\mathrm{sg}} = 1.0$ μm, the backward-emitting device, with $\Lambda_{\mathrm{sg}} = 0.8$ μm, exhibited a lower efficiency at longer wavelengths.

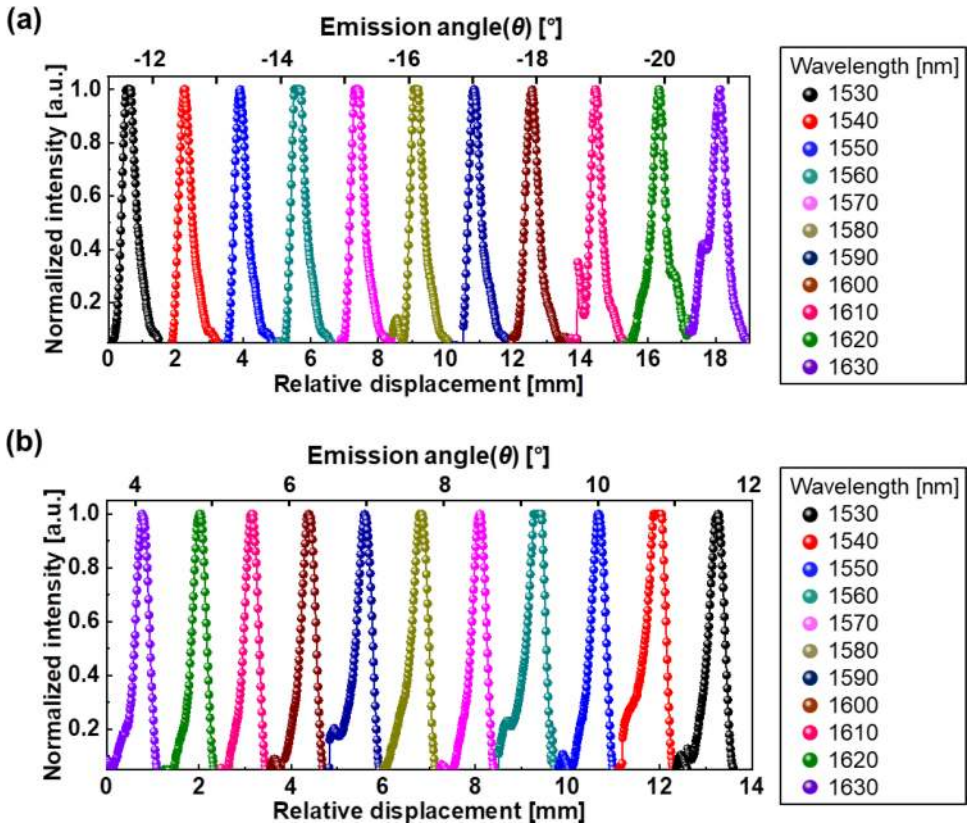

Fig. 4. Measured relative displacement in the x-direction and the corresponding emission angle of the main lobe with the wavelength for (a) the backward and (b) forward emission. The intensity profile for the beam was normalized and sequentially merged to represent displacements as observed at $d =$ 10 cm.

Therefore, the grating lobe could exhibit a higher efficiency than that of the main lobe. Note that both devices, sharing the same vertical dimension, produced disparate emission characteristics for the main and grating lobes. As depicted in polar coordinates, the angular position of the grating lobe can be identified via the longitudinal emission angle (θ) of the main lobe and the lateral angle (ψ) as determined by the channel spacing. The longitudinal angle for the grating lobe is closely related to that of the main lobe. Furthermore, the upward emission is dependent on the combination of the main and grating lobe; thus, the emission response of the latter should also be affected by the directionality of the main lobe. As a beam scanning device, the grating lobes are presumed to be substantially suppressed, relative to the main lobe, and their directionality should be stably preserved throughout the desired spectral region. As shown in Fig. 5(a), for the main lobe, the angle of diffraction (θ') in the cavity, in connection with a 2D modelled resonator inclusive of the SiN and BOX layers, is dependent on the surface grating period, in accordance with $\theta' = \sin^{-1}\{(n_{eff} - (\lambda/\Lambda_{sg}))/n_{eff}\}$. Under constant Λ_{sg} and $\mathrm{n_{eff}}$, increasing the diffraction angle of θ' will diminish the optical thickness of the antenna [22]. Moreover, a grating vector **G** leading to a higher steering efficiency makes θ' more sensitive to variations in wavelength, thus rendering the optical thickness more susceptible to variations in the wavelength. The emission characteristics of the antenna exploiting a strong grating vector was further validated with the introduction of another device for $\Lambda_{\mathrm{sg}} = 0.7$ μm.

As shown in Fig. 2(b), it was expected that an antenna with a stronger grating vector than the case of $\Lambda_{\mathrm{sg}} = 0.7$ μm may provide a steering range beyond 10° in the longitudinal direction.

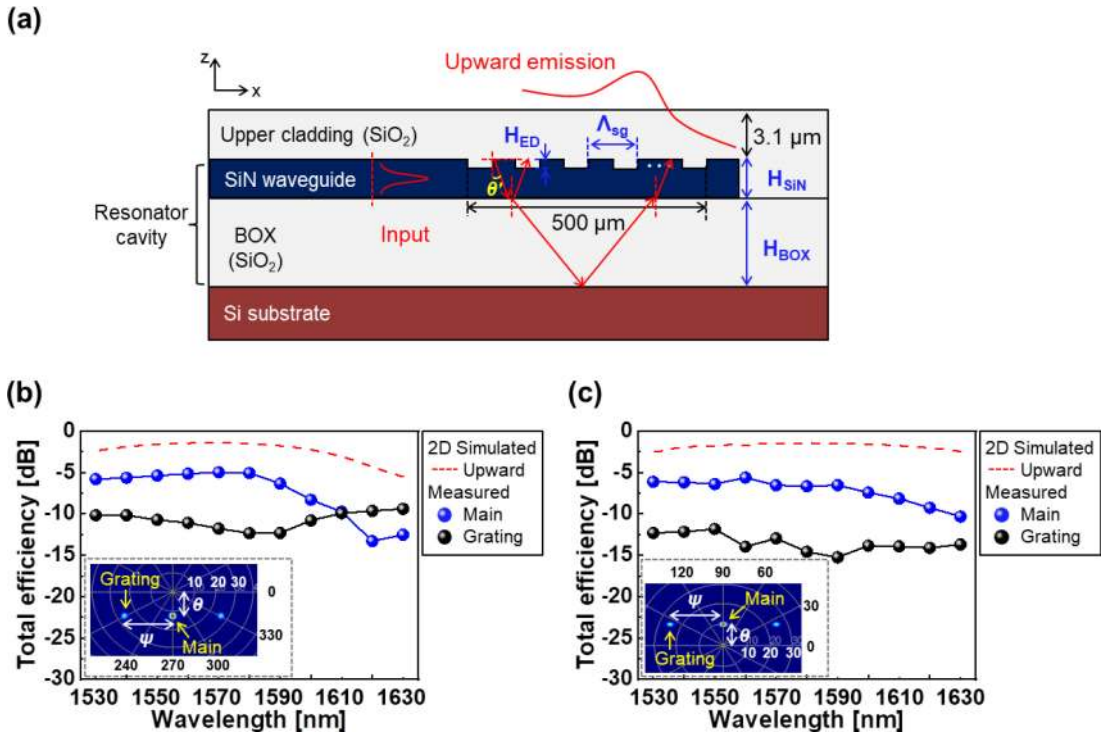

Fig. 5. (a) 2D modelled grating antenna structure to assess the upward emission. Simulated upward efficiency and measured total efficiencies of the main and grating lobes, for the two cases with (b) $\Lambda_{\mathrm{sg}} = 0.8\ \mu$m and (c) $\Lambda_{\mathrm{sg}} = 1.0\ \mu$m. Insets show the three-dimensional simulated far-field beam patterns.

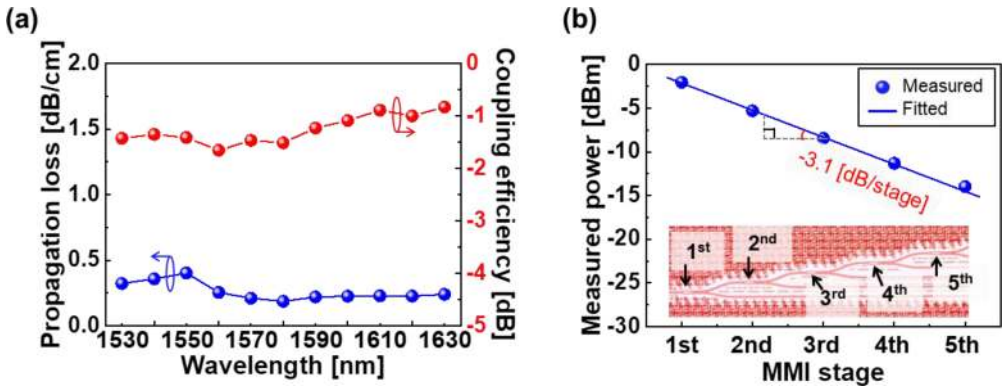

Fig. 6. (a) Measured propagation loss of the SiN waveguide and the coupling efficiency of the SSC. (b) Variations of the measured power at $\lambda = 1550$ nm for one output port of the 5-stage MMI splitter.

However, as discussed for Figs. 5(b) and 5(c), a strong grating vector would reduce the optical thickness of the SiN and BOX layers. The beam steering of the device with $\Lambda_{\mathrm{sg}} = 0.7\ \mu$m was also investigated with respect to the steering range and emission response. As shown in Figs. 7(a) and 7(b), the beam steering range was obtained for the limited wavelengths running from1530 to 1610 nm, due to the finite field-of-view of the camera; however, the emission responses of the main and grating lobes were obtained over the whole spectral region. The device was confirmed to steer the main lobe from $\theta = -27.7°$ to $-37.2°$, equating to a steering efficiency of 0.119°/nm. Enhanced

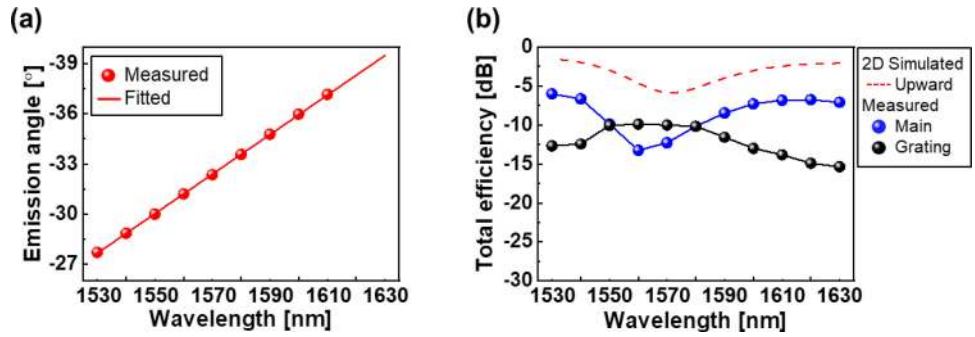

Fig. 7. (a) Measured emission angle of the main lobe for the SiN OPA tapping into a surface-relief grating period of 0.7 μm. (b) 2D simulated upward emission and measured total efficiencies of the main and grating lobes.

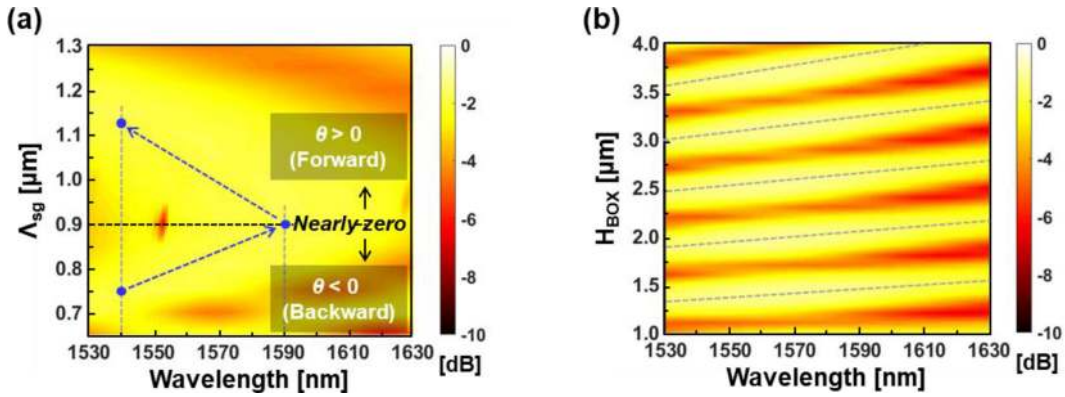

Fig. 8. (a) Simulated contour map of the upward emission spectra for a 2D modelled grating antenna, dependent on Λ_{sg}. (b) Calculated upward emission spectra of the grating antenna with $\Lambda_{sg} = 0.7$ μm, depending on the BOX thickness (H_{BOX}).

by the beam steering associated with backward emission, our proposed OPA, capitalizing on a low-index SiN waveguide could demonstrate a performance comparable to that of its Si counterpart [6]. However, the grating lobe exhibited a higher emission response efficiency at wavelengths between 1550 and 1580 nm. Compared to the case of $\Lambda_{sg} = 0.8$ μm, the region exhibiting low efficiencies shifted towards shorter wavelengths, as depicted in the simulated upward emission. A strong grating vector enhanced the beam steering efficiency, yet the diffraction angle θ' in the SiN waveguide was significantly increased to make the spectral emission shift towards shorter wavelengths, due to the resulting reduced optical thickness.

4. Analysis of the Spectral Emission of the Backward-Emitting Grating Antenna

The results obtained for the three OPA devices discussed above signify that the directionality of the antenna is crucial for effectively extending the beam steering range. We investigated the influence of the design parameters on the efficiency of wavelength-tuned beam steering. Fig. 8(a) shows a contour map of the simulated upward emission of the antenna, with Λ_{sg} varying from 0.65 to 1.3 μm. For $\Lambda_{sg} = 0.9$ μm, there was a distinct spectral emission, resulting in an efficiency of -6.4 dB around $\lambda = 1550$ nm, the emission angle of which was near-normal [9]. Based on the

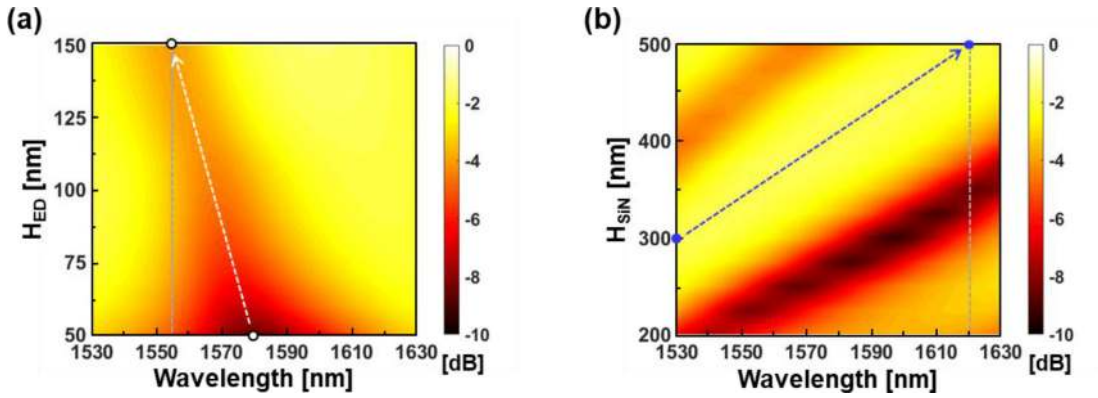

Fig. 9. Effect of (a) the etch depth (H_{ED}) and (b) the SiN waveguide thickness (H_{SiN}) on the directionality of the antenna for Λ_{sg} and H_{BOX} of 0.7 μm and 4.0 μm, respectively.

case of $\Lambda_{sg} = 0.9$ μm leading to near-normal emission, the direction for the peak wavelength (blue dot) shift was inverted, as indicated by the dashed line. Owing to a strong grating vector, the peak wavelength changed more rapidly for the backward beam emission. A higher wavelength sensitivity in the diffraction angle θ' caused the emission response more responsive to Λ_{sg}. With decreasing Λ_{sg}, the yellow region, indicating an efficiency higher than -2 dB, narrows, implying that the spectral emission response is more sensitive to variations in wavelength. The wavelength dependency of the spectral emission may be abated by adjusting the thicknesses of the BOX and SiN layers [18], [23], [24]. Hence, we particularly explored the emission response for the case of $\Lambda_{sg} = 0.7$ μm, for a varying BOX layer thickness (H_{BOX}). As shown in Fig. 8(b), a periodic response was observed, with respect to H_{BOX}. However, the yellow region is tilted with respect to H_{BOX}, thus deteriorating the response over the desired spectral region. For $H_{BOX} = 2.0$ or 2.6 μm, the SiN OPA provides a stable emission characteristic over a broad spectral band for the case of $\Lambda_{sg} = 0.7$ μm. The effect of the etch depth (H_{ED}) and the SiN thickness (H_{SiN}) on the directionality was then examined for $\Lambda_{sg} = 0.7$ μm and $H_{BOX} = 4.0$ μm. As shown in Figs. 9(a) and 9(b), the effects of H_{ED} and H_{SiN} were investigated separately, with H_{SiN} and H_{ED} fixed at 500 nm and 100 nm, respectively. The minimum efficiency increased with an increasing H_{ED}, and the corresponding wavelength, indicated by the white dot, shifted towards shorter wavelengths along the dashed line. H_{ED} should preferably be increased only to a value for which the divergence angle in the longitudinal direction would not be exacerbated. Moreover, a larger H_{SiN} value shifted the peak wavelength (the blue dot) of the emission towards longer wavelengths. It is noted that the adjustment of H_{ED} and H_{SiN} is limited, relative to H_{BOX}.

5. Conclusion

A backward-emitting SiN OPA, incorporating a strong grating vector for a surface-relief grating, was proposed to mitigate the limited steering efficiency of the SiN waveguide grating antenna. Two backward-emitting devices, with $\Lambda_{sg} = 0.8$ and 0.7 μm, were prepared and their respective beam steering was thoroughly scrutinized by via a comparison with a forward-emitting case, using $\Lambda_{sg} = 1.0$ μm. The beam steering of the prepared OPAs was examined, based on the steering range and the directionality of the antenna for wavelengths ranging from 1530 to 1630 nm. The two devices exploiting $\Lambda_{sg} = 0.8$ and 0.7 μm exhibited steering efficiencies 27% and 60% higher than that of the device using $\Lambda_{sg} = 1.0$ μm, respectively. However, the grating vector, providing a higher steering efficiency, made the directionality of the antenna more sensitive to variations in wavelength, owing to a higher wavelength sensitivity in the optical thickness of the antenna. By investigating the impact of Λ_{sg} and H_{BOX} on the directionality, for the case using $\Lambda_{sg} = 0.7$ μm, it

was determined that a thinner H_{BOX} may alleviate the influence of a strong grating vector on the optical thickness of the antenna, thus securing the effective steering range of a backward-emitting OPA. We further inspected the directionality of the antenna, with respect to the etch depth and the SiN core thickness. The proposed design scheme will improve the feasibility of SiN OPAs in creating highly efficient solid-state LiDAR.

Acknowledgment

The authors are grateful to Ligentec for device fabrication and to Dr. Chang-Joon Chae from the Agency for Defense Development and Dr. Young-Ho Kim and Dr. Sung-Yong Ko from i3system, Inc. for helpful discussions.

References

[1] M. J. R. Heck, "Highly integrated optical phased arrays: Photonic integrated circuits for optical beam shaping and beam steering," *Nanophotonics*, vol. 6, no. 1, pp. 93–107, 2017.
[2] C. V. Poulton *et al.*, "Long-range LiDAR and free-space data communication with high-performance optical phased arrays," *IEEE J. Sel. Top. Quantum Electron.*, vol. 25, no. 5, Sep./Oct. 2019, Art. no. 7700108.
[3] S. H. Kim *et al.*, "Thermo-optic control of the longitudinal radiation angle in a silicon-based optical phased array," *Opt. Lett.*, vol. 44, no. 2, pp. 411–414, 2019.
[4] Y. Zhang *et al.*, "Sub-wavelength-pitch silicon-photonic optical phased array for large field-of-regard coherent optical beam steering," *Opt. Express*, vol. 27, no. 3, pp. 1929–1940, 2019.
[5] D. N. Hutchison *et al.*, "High-resolution aliasing-free optical beam steering," *Optica*, vol. 3, no. 8, pp. 887–890, 2016.
[6] J. C. Hulme *et al.*, "Fully integrated hybrid silicon two dimensional beam scanner," *Opt. Express*, vol. 23, no. 5, pp. 5861–5874, 2015.
[7] D. Kwong *et al.*, "On-chip silicon optical phased array for two-dimensional beam steering," *Opt. Lett.*, vol. 39, no. 4, pp. 941–944, 2014.
[8] J. K. Doylend, M. J. R. Heck, J. T. Bovington, J. D. Peters, L. A. Coldren, and J. E. Bowers, "Two-dimensional free-space beam steering with an optical phased array on silicon-on-insulator," *Opt. Express*, vol. 19, no. 22, pp. 21595–21604, 2011.
[9] K. Van Acoleyen, W. Bogaerts, J. Jágerská, N. L. Thomas, R. Houdré, and R. Baets, "Off-chip beam steering with a one-dimensional optical phased array on silicon-on-insulator," *Opt. Lett.*, vol. 34, no. 9, pp. 1477–1479, 2009.
[10] Y. Gao *et al.*, "High-power, narrow-linewidth, miniaturized silicon photonic tunable laser with accurate frequency control," *J. Lightw. Technol.*, vol. 38, no. 2, pp. 256–271, Jan. 2020.
[11] A. Rahim *et al.*, "Expanding the silicon photonics portfolio with silicon nitride photonic integrated circuits," *J. Lightw. Technol.*, vol. 35, no. 4, pp. 639–649, Feb. 2017.
[12] N. Suzuki, "FDTD analysis of two-photon absorption and free-carrier absorption in Si high-index-contrast waveguides," *J. Lightw. Technol.*, vol. 25, no. 9, pp. 2495–2501, Feb. 2007.
[13] D. J. Moss, R. Morandotti, A. L. Gaeta, and M. Lipson, "New CMOS-compatible platforms based on silicon nitride and Hydex for nonlinear optics," *Nat. Photon.*, vol. 7, no. 8, pp. 597–607, 2013.
[14] P. Muñoz *et al.*, "Silicon nitride photonic integration platforms for visible, near-infrared and mid-infrared application," *Sensors*, vol. 17, no. 9, 2017, Art. no. 2088.
[15] C. V. Poulton *et al.*, "Large-scale silicon nitride nanophotonic phased arrays at infrared and visible wavelengths," *Opt. Lett.*, vol. 42, no. 1, pp. 21–24, 2017.
[16] A. Arbabi and L. L. Goddard, "Measurements of the refractive indices and thermo-optic coefficients of Si3N4 and SiOx using microring resonances," *Opt. Lett.*, vol. 38, no. 19, pp. 3878–3881, 2013.
[17] N. A. Tyler *et al.*, "SiN integrated optical phased arrays for two-dimensional beam steering at a single near-infrared wavelength," *Opt. Express*, vol. 27, no. 4, pp. 5851–5858, 2019.
[18] C. S. Im, B. Bhandari, K. P. Lee, S. M. Kim, M. C. Oh, and S. S. Lee, "Silicon nitride optical phased array based on a grating antenna enabling wavelength-tuned beam steering," *Opt. Express*, vol. 28, no. 3, pp. 3270–3279, 2020.
[19] T. Komljenovic, R. Helkey, L. Coldren, and J. E. Bowers, "Sparse aperiodic arrays for optical beam forming and LIDAR," *Opt. Express*, vol. 25, no. 3, pp. 2511–2528, 2017.
[20] D. Kwong, A. Hosseini, Y. Zhang, and R. T. Chen, "1 x 12 Unequally spaced waveguide array for actively tuned optical phased array on a silicon nanomembrane," *Appl. Phys. Lett.*, vol. 99, no. 5, 2011, Art. no. 051104.
[21] D. Vermeulen *et al.*, "High-efficiency fiber-to-chip grating couplers realized using an advanced CMOS-compatible silicon-on-insulator platform," *Opt. Express*, vol. 18, no. 17, pp. 18278–18283, 2010.
[22] H. A. Macleod, *Thin-Film Optical Filters*. 4th ed. Boca Raton, Florida, USA: CRC Press, 2010, Chapter 2.
[23] S. Romero-García, F. Merget, F. Zhong, H. Finkelstein, and J. Witzens, "Silicon nitride CMOS-compatible platform for integrated photonics applications at visible wavelengths," *Opt. Express*, vol. 21, no. 12, pp. 14036–14046, 2013.
[24] A. Z. Subramanian, S. Selvaraja, P. Verheyen, A. Dhakal, K. Komorowska, and R. Baets, "Near-infrared grating couplers for silicon nitride photonic wires," *IEEE Photon. Technol. Lett.*, vol. 24, no. 19, pp. 1700–1703, Oct. 2012.